An investigation of dynamic vehicle-bridge interaction effects based on a comprehensive set of trains and bridges

Antonia M. Kohl, Kim-Denise Clement, Jens Schneider

Technical University of Darmstadt, Darmstadt, Germany

Andrei Firus

iSEA Tec GmbH, Friedrichshafen, Germany

Geert Lombaert

KU Leuven, Leuven, Belgium

Abstract

The consideration of interaction effects between vehicle and structure is an important aspect in the dynamic analysis of railway bridges. They usually lead to a reduction of the structural responses compared to computations without consideration of the vehicle-bridge interaction. The interaction effects can either be accounted for by Finite Element analysis including multi-body models of the vehicles or in a simplified way - as adopted by the actual regulations - by artificially increasing the bridge damping. In this way, a simplified dynamic analysis under consideration of the interaction effects is possible using the moving load model.

However, several studies have shown that the current approach of the additional damping included in Eurocode 1 is non-conservative in many cases, possibly leading to an underestimation of the structural responses. The approach in Eurocode 1 as well as the more recently proposed approaches were based on a limited number of combinations of trains and bridges. In order to verify these approaches in a more thorough way,the present paper investigates the vehicle-bridge interaction effects based on 25 real high-speed passenger trains (including conventional and articulated trains) and over 100 single-span bridges with spans ranging from 5 m to 55 m.

A typical criterion of analyzing the vehicle-bridge interaction phenomenon is the reduction of the structural acceleration computed using a 2D multi-body representation of the vehicle compared to the simplified moving load approach. Therefore, the reduction of the acceleration due to the interaction is discussed in detail and put in relation to the results of previous research. The results of over 800 000 dynamic analyses performed in the present study confirm that the additional

damping approach depending on the bridge span as included in Eurocode 1 overestimates the actual vehicle-bridge interaction effects. Furthermore, the results show that recent additional damping approaches depending on bridge and train characteristics lead to more reliable additional damping values. Their application requires public availability of train characteristics and an extension of the approaches for articulated as well as heterogeneous trains.
Keywords: bridge dynamics, railway bridges, train crossing, vehicle-bridge interaction, moving loads, multi-body models, additional damping value

1. Introduction

In general, the dynamic analysis of railway bridges under a train passage is based on a moving load model (MLM). In the MLM, the train is represented by a set of point forces, corresponding to the static axle loads of the vehicle, which are moving over the structure at a constant speed. This is considered as a rather conservative approach, since it neglects the well-known (mostly) positive effects of the vehicle-bridge interaction (VBI). These effects arise mainly due to the energy dissipated by the vehicle mechanisms and the energy transfer from one subsystem to another as in the case of a tuned mass damper [1]. In this context, it has already been reported in the literature, that the VBI effect is most pronounced in case of a resonance excitation [2].

Nevertheless, the MLM approach requires a much lower computational effort compared to computations based on multi-body models (MBMs) for the representation of the VBI and are therefore usually preferred in practice. In addition, the parameters of the MBMs are only publicly available for a limited number of trains, so that a calculation considering the interactions is only possible for these trains.

In order to take the beneficial effects of VBI into account in an analysis based on the MLM, Eurocode 1 (EC 1) [3] and the German guideline RIL 804 [4] present the additional damping method (ADM), where the damping of the (empty) bridge is artificially increased, so that the results of the MLM match with those incorporating VBI. The ADM was established in 1999 by the European Rail Research Institute (ERRI) [5] based on calculations considering only two vehicles (ICE 2 and Eurostar, i.e. typical high-speed trains at that time) and ten simply supported bridges (see table 1

Email address: kohl@ismd.tu-darmstadt.de (Antonia M. Kohl, Kim-Denise Clement, Jens Schneider)

in [5]). The interaction effects were evaluated by means of a simplified interaction model and the additional damping $\Delta\xi_{\mathrm{ADM}}$ is expressed as a function of the bridge span L [5].

As previously shown by Arvidsson and Karoumi [6], the additional damping $\Delta\xi_{\mathrm{ADM}}$ leads to non-conservative results in certain cases. Several calculations with detailed interaction models and different train-bridge combinations lead to lower additional damping values than the value of $\Delta\xi_{\mathrm{ADM}}$ provided in EC 1 [3]. Therefore, the elimination of the additional damping from European standards is currently considered. However, without applying the additional damping $\Delta\xi_{\mathrm{ADM}}$, a number of existing structures may no longer meet the design criteria. This issue arises partly due to the fact that they were designed under consideration of load models, which are not fully compliant with the current ones and do not even entirely cover the current traffic load characteristics. This means that the reserves of the structural capacity are already exploited due to the traffic development. As a result, any structural reserve, however small, such as the additional damping, becomes highly significant in the verification of existing structures.

Considering the previously mentioned difficulties, i.e. the ADM being non-conservative in some situations but needed when verifying existing bridges, a new, more reliable and conservative formulation of the additional damping is clearly needed. In this sense, some researchers have already made first attempts towards a redefined additional damping $\Delta\xi$. Doménech et al. [2] suggested to not only consider the bridge span L when defining the additional damping, but also defined the bridge-to-vehicle ratios of length, frequency and mass. The dependency of the additional damping $\Delta\xi$ on the ratios defined by Doménech et al. [2] is further discussed in section 6.3. In this approach, the additional damping $\Delta\xi$ results from an iterative process, which seeks to match the result of the dynamic analysis of a train passage by means of MLM close to the corresponding result obtained under consideration of the interaction by using a MBM of the vehicle. This means that the additional damping is here defined as a tuning parameter, as it was done by the ERRI [5] and also in the present study.

Another possibility is to define the additional damping by considering the mechanical interaction problem like Yau et al. [7] and Stoura and Dimitrakopulous [8]. These works investigated the additional damping by considering the mechanical properties of train and bridge and propose analytic expressions derived from the mechanical characteristics (see section 7).

Even though the studies of [2, 7, 8] are based on strong and well justified research hypotheses,

they have at this point only been verified for a limited set of bridges and trains. The present study tackles this issue and analyzes the additional damping based on a very comprehensive set of about 100 bridge structures and 25 vehicles. A total of about 800 000 passages were computed both using the MLM and the MBM approaches, allowing thus a comprehensive analysis of the additional damping for realistic train-bridge combinations. This is performed by means of the loosely coupled iterative algorithm provided by Liu et al. [9].

Besides the maximum structural acceleration defining the additional damping $\Delta\xi$, this paper discusses another influence factor of the VBI, which is defined as the additional mass $\Delta\mu$. The influence of the additional mass is described in subsection 5.6 and leads to an increased bridge stiffness and therefore a reduction of the resonance speed.

2. Train data set and model description

This section describes the database for the trains that was used in the present study. More details about the MBMs of the trains included in this study are available in a repository online [10].

The train data set contains 14 conventional and 11 articulated high-speed passenger trains.

2.1. Conventional trains

The 14 conventional trains with two bogies per car body (see Figure 1) include the following trains with characteristics found in the literature: Alfa Pendular [11], ETR500Y [12], Green train [13], Pioneer train [14], Railjet [15], ICE 2 [5], and ICE 4 [16]. In this respect it is to be mentioned that the mass data of the ICE 4 provided in [16] was adjusted after consultations with the vehicle manufacturer.

In addition, the collection of MBMs was extended by two more versions of the ICE 2, which were defined in consultation with Siemens and DB Fernverkehr AG. They represent the currently operating configurations of the ICE 2, which include only eight (instead of 14) car bodies.

Moreover, two modified models of the ICE 4 were defined for the load cases MU (axle load at "Design mass in working order") and MND (axle load at "Normal design payload").

Finally, the database is completed by a MBM for the ICE-S from information given by DB AG as well as two representative conventional high-speed train models from further vehicle manufacturers, referred to as "HS conventional".

2.2. Articulated trains

The 11 articulated trains (with shared bogies between the central car bodies, see Figure 2) include the following trains found in the literature: AVE S-100 [17], two versions of the Eurostar [5, 18], KHST [19], TGV [20], and Thalys [18]. In this respect it is to be mentioned that the moments of inertia of the Thalys train provided in [18] were multiplied by a factor of 10^3, since the original values are unrealistically small.

The collection of articulated MBMs was extended by five additional MBMs for trains from further vehicle manufacturers. These include three MBMs for an EuroCity (measured loads and load cases MU and MND) and two electric multiple unit (EMU) trains with three and four carriages. The data for these additional MBMs is not published in the previously mentioned repository, because of their confidential character. Nevertheless, the trains are included in the results presented within the present paper.

2.3. Multi-body models

Within the present work, the two previously mentioned vehicle types (conventional and articulated trains) are modeled as two-dimensional MBMs (see Figures 1 and 2). These models are similar to the detailed interaction models used by ERRI [5] as well as more recent publications [2, 11, 12, 21–24].

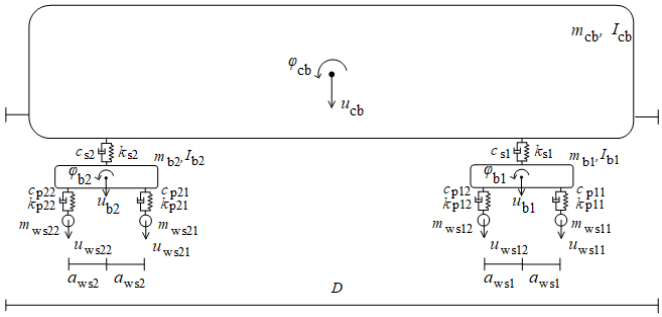


Figure 1: Six degree-of-freedom 2D multi-body model of a conventional car

Each conventional car has two bogies and the corresponding 2D MBM has six degrees of freedom (DOFs) $\mathbf{U}_\mathrm{v} = [u_{\mathrm{b}1}, \varphi_{\mathrm{b}1}, u_{\mathrm{cb}}, \varphi_{\mathrm{cb}}, u_{\mathrm{b}2}, \varphi_{\mathrm{b}2}]^\mathrm{T}$.

It is to be mentioned that no vertical connection between neighbouring conventional car bodies is considered. As shown in Figure 1, four springs and dampers connect the wheels and bogies on the primary level (k_p and c_p) and two springs and dampers connect the bogies to the car body on

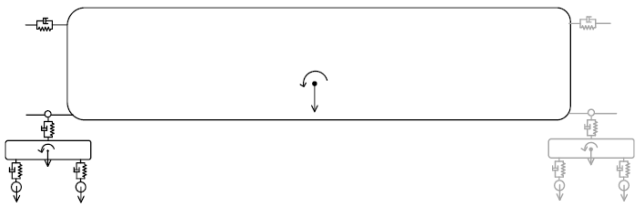


Figure 2: Four degree-of-freedom 2D multi-body model of a central car with articulated bogies

the secondary level (k_s and c_s). Although the train suspension generally behaves in a non-linear fashion, it is modeled here by a set of linear springs and dampers considering a linearized behaviour as is customary in train-bridge interaction studies. [2, 5–9, 11, 12, 14, 15, 17–28]

Articulated trains consist of two side cars and multiple central cars, which share an articulated bogie with their neighbouring car body. Some articulated trains additionally have conventional traction cars attached to the side cars. In contrast to the conventional vehicle model, the neighbouring car bodies with articulated bogies are vertically connected to each other as well as to the shared bogie (see Figure 2). Additionally, articulated train models feature horizontal pitching dampers between the neighbouring car bodies, which are also included in the definition of the MBMs and illustrated in Figure 2.

2.4. Investigation of model parameters

For each train from the data set, all necessary parameters of the MBM were defined. The primary and secondary stiffness and damping parameters and the masses of all car bodies, bogies and wheel sets as well as the moments of inertia of car bodies and bogies were collected and assigned to the elements of the MBM.

The model parameters (see Figure 3) for the bogies of the MBMs of all 25 investigated trains are shown in the boxplots given in Figure 5 in boxplot representations. Boxplots demonstrate the spread of numerical data through their quartiles [29] and also display outliers, which differ significantly from the data set [30]. The allocation of the parameters to the train models can be found at [10].

In [10] and Figure 5, the parameters of the MBMs – except for bogie masses, car body masses, and moments of inertia – are evaluated separately for each side of the vehicle and are to be multiplied by two, in order to obtain the parameters for the simplified 2D modeling approach (see Figure 3).

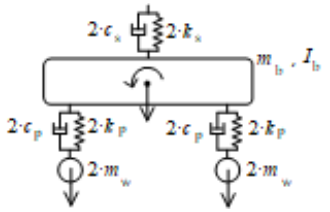


Figure 3: Model parameters for bogies

Moreover, some articulated bogies have two secondary springs over each rail (see Figure 4 left). In the parameter definition, these are already replaced by values for a single equivalent spring and damper, so that all bogies are defined as illustrated in Figure 4 right.

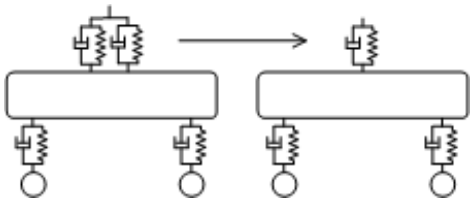


Figure 4: Equivalent secondary spring for articulated bogies with two secondary springs

As shown in Figure 2, articulated car bodies are connected by horizontal pitching dampers, which were mostly not included in the information from the manufacturers and are therefore not explicitly presented in the boxplots. The horizontal damping values were assumed as 12 MNs/m at a distance of 3 m to the center of gravity of the car body, if not otherwise specified.

Figure 5 illustrates the ranges of parameters for the MBMs. On top of the boxplots, the explicit values of ICE 2 and Eurostar, considered when defining the ADM of EC 1 [3], are superimposed in order to situate the characteristics of these two vehicle types with respect to the parameter range of the train collection.

Figure 5a shows the masses of all bogies that are included in the MBMs. The bogie masses are divided into conventional ($m_{\mathrm{b,con.}}$) and articulated ($m_{\mathrm{b,art.}}$). Since not all bogies of one individual train have the same characteristics, 61 bogie masses are included in the boxplot. Furthermore, it is to be mentioned, that it was not possible to make a distinction between the masses of the powered and unpowered bogies, as this information was not available for all MBMs. The bogie masses of conventional trains have a median of about 3 tons and the bogie masses of articulated trains have a median of about 3.8 tons (see Figure 5a), while the mass of half a wheel set is about 1 ton (i.e. 2 tons for the total unsprung mass of a wheel set), see Figure 5b.

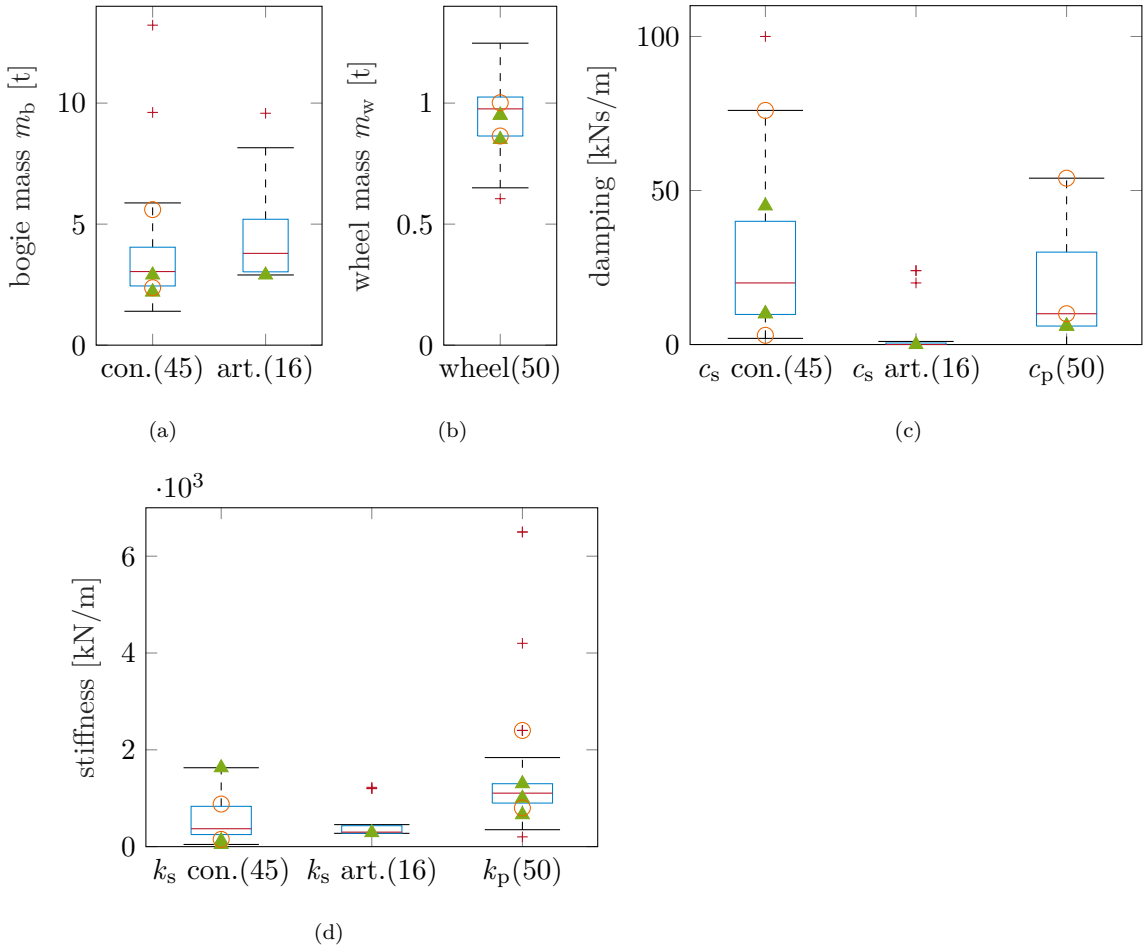


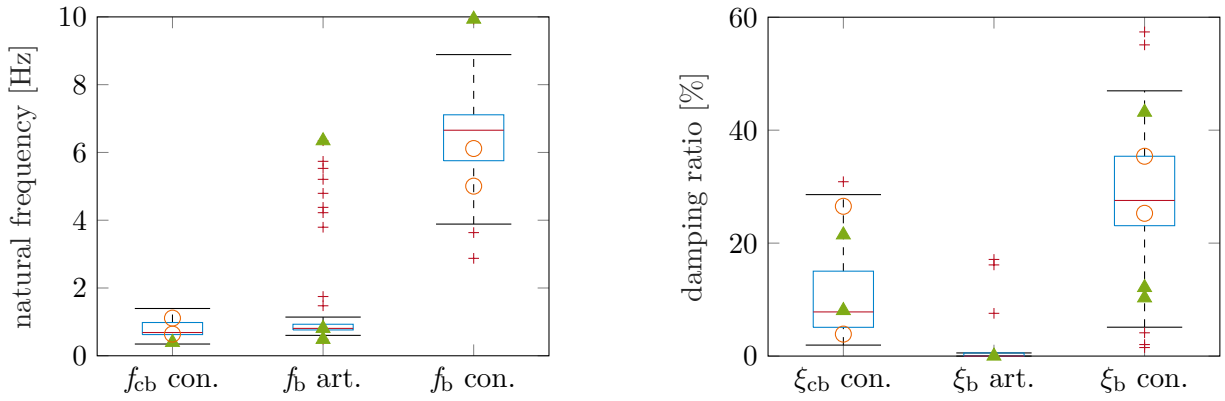
Figure 5: Boxplots of the train parameters (number of bogies with different characteristics from 25 train models given in brackets): min/max (——), 25-/75-percentile (——), median (——), outliers (+); separate marks for trains used by ERRI [5]: Eurostar (▲), ICE 2 (○); (a): bogie mass for conventional and articulated trains; (b): wheel mass (1/2 wheel set); (c): secondary damping (conventional bogie, articulated bogie) and primary damping per element; (d): secondary stiffness (conventional bogie, articulated bogie) and primary stiffness per element

The outlier of the bogie mass at about 13 tons corresponds to the powered bogie traction car of the Railjet. The reason for this is that this bogie is also used for heavy freight trains, as indicated by the manufacturer. It also leads to the outlier in the secondary damping of conventional bogies (see Figure 5c). The second outlier of the conventional bogie mass at about 10 tons corresponds to the powered bogie of the ICE-S. The outlier for the articulated train corresponds to the Eurostar with the parameters given by Kouroussis et al. [18]. The conventional bogie masses of the Eurostar defined by the ERRI [5] are situated around the median and around the 25-percentile, while the articulated bogie mass lies close to the minimum which is here about the same as the 25-percentile. The bogie masses of the ICE 2 defined by the ERRI [5] both lie within the 25- to 75-percentiles of the train collection. Therefore, it can be stated that the bogie masses of both vehicles considered by the ERRI [5] are representative for the comprehensive parameter set collected within this work.

This is also valid for the wheel set masses. The masses of half a wheel set of the Eurostar and the ICE 2 lie between the 25- and 75-percentile values, at around 0.8 t to 1 t. This can be seen in the boxplot shown in Figure 5b, which was generated based on 50 wheel masses (m_{w}).

Similar to the bogie masses, the secondary damping c_{s} (see Figure 5c) and stiffness k_{s} (see Figure 5d) are also compared separately for conventional and articulated bogies, while the primary stiffness k_{p} and damping c_{p} values are aggregated for all trains. To understand the values correctly, it is important to note - as already mentioned - that they are displayed per element as they occur in reality in 3D. Therefore, they have to be multiplied by 2, in order to determine the parameters of the 2D MBM (see Figure 3).

The damping values in Figure 5c display a high variability. The median of the secondary damping for conventional bogies is about 20 kNs/m, while most articulated bogies have no secondary damping. The median primary damping value is about 10 kNs/m. As previously mentioned, the outlier in the secondary damping of conventional bogies corresponds to the powered bogie belonging to the traction car of the Railjet. The secondary damping values of the conventional bogie of the Eurostar [5] are around the 25- and 75-percentile, while the articulated bogie does not have a secondary damper as it is the case for most articulated bogies. The secondary damping of the ICE 2 [5] sticks to the lower and upper limit of the parameter set collected in this work. Regarding the primary dampers, the highest value is found for ICE 2 [5] as well as the median. The primary damping value of the Eurostar [5] is around the 25-percentile. Considering the fact that higher and lower



(a) (b)

Figure 6: Boxplots of the modal train characteristics: min/max (——), 25-/75-percentile (——), median (——), outliers (+); separate marks for trains used by ERRI [5]: Eurostar (▲), ICE 2 (○); (a): natural frequency of the vertical bouncing modes for car body (f_{cb}) and bogie (f_b); (b): damping ratio of the vertical bouncing modes for car body (ξ_{cb}) and bogie (ξ_b)

values are both included in the MBMs of the Eurostar and ICE 2 considered by the ERRI [5], the damping parameters still seem to fit to the ranges given by the present collection.

In Figure 5d, it can be seen that the median secondary stiffness of both kinds of bogies is below 0.5 MN/m and the median primary stiffness is about 1 MN/m. As for the damping values, the secondary stiffnesses of the Eurostar and ICE 2 [5] seem to fit well with the values from the other trains in the collection. One of the outliers of the primary stiffness corresponds to the powered bogies of the ICE 2 [5], while the second outlier is also caused by a powered bogie of the ICE vehicle family. The highest outlier of primary stiffness results from the unpowered bogie of the ICE 4.

To better understand the resulting characteristics of the train data presented in Figure 5, the natural frequency of the vertical car body and bogie bouncing modes as well as the damping ratios of these modes are shown in Figure 6. The natural frequency of the vertical car body (f_{cb}) and bogie (f_b) bouncing modes were determined from the solution of the generalized eigenvalue problem defined by the stiffness and mass matrix of the carriage as modeled in Figure 1. The damping ratios (ξ_{cb} and ξ_b) additionally depend on the damping matrix and were calculated from the modal damping and mass, as described in [1].

Figure 6a shows the natural frequency of the vertical bouncing modes for car body and bogie. The natural frequency of the vertical bouncing mode can only be calculated for conventional car

bodies, since the central cars of articulated trains are vertically connected and can therefore not be treated individually. For the comparison to previous research in section 7, the most frequent value of each train was chosen. There are even higher values for the natural frequency of the conventional bogie bouncing modes that are not presented in figure 6a. This includes 17.29 Hz for ICE 4 (measured), which is caused by the high primary stiffness k_p of 6500 kN/m. The frequencies of ICE 2 [5] fit well with the values from the other trains in the collection while the Eurostar [5] has a wide range of natural frequencies, due to the wide range secondary stiffnesses k_s.

Figure 6b shows the damping ratio of the vertical bouncing modes for car body and bogie. The damping ratios of the ICE 2 and the Eurostar [5] fit well with the values from the other trains in the collection. The low damping ratio of the articulated bogies can be explained by the low secondary damping of the articulated trains, see Figure 5c.

3. Bridge data sets

As previously mentioned, over 100 single-span bridges were considered in the calculations. For the calculations of train crossings, the bridge structures were modeled as simply supported Euler-Bernoulli beams, see Figure 7. The Finite Element (FE) bridge models are defined by their bridge span L, mass distribution μ, bending stiffness EI, stiffness category w/L (ratio maximum deflection to bridge span), and modal damping ratio ξ_br.

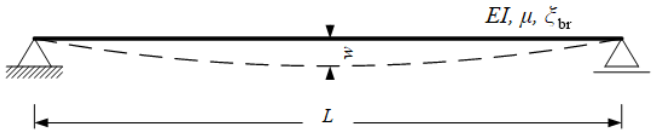


Figure 7: Beam model of a single-span bridge

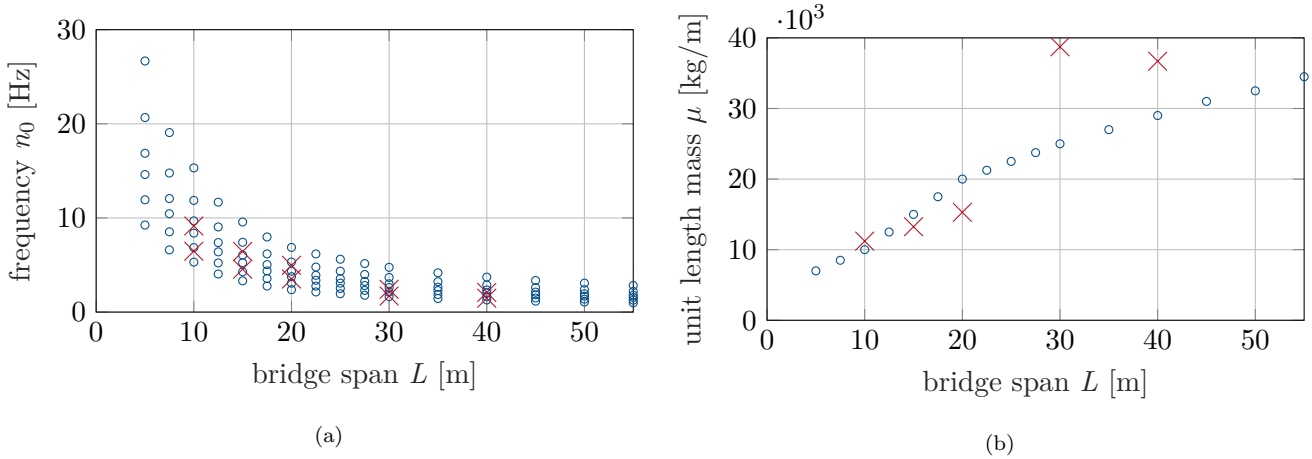
They include a set of ten bridges which have been taken from table 1 in ERRI RP 4 [5] and are referred to as bridge set A, as well as 96 bridges based on table 6 in ERRI RP 4 [5], which are referred to as bridge set B. Bridge set A is the bridge set used in the determination of the ADM of EC 1 [3] respectively RIL 804 [4] while set B is an extension of further bridges included in ERRI RP 4 [5].

Figure 8a shows the variation of bridge eigenfrequencies dependent on the bridge span L. Similar to ERRI RP 4 [5] table 6, the mass per unit length for bridge set B was defined as a function of

the span and takes values between 7 t/m and 34.5 t/m, see Figure 8b. Figure 8b shows a smaller number of values than Figure 8a, because the bridges of the same span have the same mass per unit length for both bridge sets.

The spans of the bridges range from 5 m to 55 m and the modal damping ratio is defined as 1.5 % for bridge set B and 1.0 % for bridge set A.

A list of all bridges and their characteristics is available at [10].



(a) (b)

Figure 8: Bridge set A(×; table 1 in [5]) and bridge set B (○; based on table 6 in [5]): (a) bridge frequency, (b) bridge mass per unit length

4. Computation method

In order to calculate the bridge response due to a train crossing, the subsystem of the train is modeled as a MBM (see section 2) and the bridge subsystem is modeled as a simply supported Euler-Bernoulli beam (see section 3). These two subsystems are coupled, to take into account the VBI occurring during the train crossing. A perfect contact between wheels and rails is assumed and the calculations are performed with the loosely coupled iterative algorithm provided by Liu et al. [9].

4.1. Equations of motion

The equations of motion of the vehicle and bridge are solved separately and are given by:

$$\begin{aligned} \mathbf{M}_\mathrm{v}\ddot{\mathbf{U}}_\mathrm{v} + \mathbf{C}_\mathrm{v}\dot{\mathbf{U}}_\mathrm{v} + \mathbf{K}_\mathrm{v}\mathbf{U}_\mathrm{v} &= \mathbf{P}_\mathrm{v}, \\ \mathbf{M}_\mathrm{b}\ddot{\mathbf{U}}_\mathrm{b} + \mathbf{C}_\mathrm{b}\dot{\mathbf{U}}_\mathrm{b} + \mathbf{K}_\mathrm{b}\mathbf{U}_\mathrm{b} &= \mathbf{P}_\mathrm{b} \end{aligned} \tag{1}$$

where $\mathbf{M}$, $\mathbf{C}$, and $\mathbf{K}$ denote the mass, damping and stiffness matrix of the vehicle (subscript v) respectively bridge (subscript b) while $\mathbf{U}$, velocity $\dot{\mathbf{U}}$, and acceleration $\ddot{\mathbf{U}}$ represent the corresponding displacement, velocity, and acceleration vector and $\mathbf{P}$ represents the load vector.

The equation of motion of the bridge is solved using the modal superposition principle [1] while the equation of motion of the vehicle is solved with direct integration.

The displacements at the contact points between wheel sets and rail are used to couple the subsystems:

$$\mathbf{U}_{\mathrm{v}}^{\mathrm{contact}}(t) = \mathbf{U}_{\mathrm{b}}^{\mathrm{contact}}(t) \tag{2}$$

The wheel sets on the bridge are selected from the displacement vector of the train $\mathbf{U}_{\mathrm{v}}^{\mathrm{contact}}(t)$. For each wheel set on the bridge, the displacement of the rail at the contact point $\mathbf{U}_{\mathrm{b}}^{\mathrm{contact}}(t)$ is calculated from the neighbouring nodes in the FE model of the bridge. For the compatibility of the displacements between the train and the track, a point contact between the two systems is assumed. The load transferred from the train to the track is distributed as it is discussed in more detail in subsection 5.5.

The load vector of the bridge $\mathbf{P}_{\mathrm{b}}$ can be determined according to

$$\mathbf{P}_{\mathrm{b}}(t) = \mathbf{P}_{\mathrm{b}}^{\mathrm{stat}}(t) + \mathbf{P}_{\mathrm{b}}^{\mathrm{dyn}}(t) \tag{3}$$

from the static and dynamic components of the load, which are determined from the train properties and motion quantities.

The load vector of the train $\mathbf{P}_{\mathrm{v}}$ is a column vector of the load vectors of all carriages including the loads for all DOFs of each carriage $\mathbf{P}_{\mathrm{carriage}} = [P_{u,\mathrm{b1}}, P_{\varphi,\mathrm{b1}}, P_{u,\mathrm{cb1}}, P_{\varphi,\mathrm{cb1}}, P_{u,\mathrm{b2}}, P_{\varphi,\mathrm{b2}}]^{\mathrm{T}}$.

4.2. Loosely coupled iterative algorithm

The two equations of motion (1) are solved separately in time domain following an iterative approach to ensure the coupling between the vehicle and the bridge. According to Liu et al. [27], the positions of the wheel sets on the bridge need to be determined and initial values ($t = t_0$) are assigned to the displacement $\mathbf{U}_{\mathrm{v}}^0$, velocity $\dot{\mathbf{U}}_{\mathrm{v}}^0$, and acceleration $\ddot{\mathbf{U}}_{\mathrm{v}}^0$ of the train and the displacement $\mathbf{U}_{\mathrm{b}}^0$, velocity $\dot{\mathbf{U}}_{\mathrm{b}}^0$, and acceleration $\ddot{\mathbf{U}}_{\mathrm{b}}^0$ of the bridge.

This is followed by an iterative process, which departs from the converged results at the previous time step t. In each iteration loop, a first estimation of accelerations $\ddot{\mathbf{U}}_{\mathrm{v},0}$ and $\ddot{\mathbf{U}}_{\mathrm{b},0}$ at time $t + \Delta t$

for the train and the bridge is assumed as the accelerations from the previous time step t. For the next time step, the new position of the wheel sets at time $t + \Delta t$ is determined here assuming the constant crossing speed v of the train.

Using the Newmark-β method [1], the velocities $\dot{\mathbf{U}}_\mathrm{v}$ and $\dot{\mathbf{U}}_\mathrm{b}$ and displacements $\mathbf{U}_\mathrm{v}$ and $\mathbf{U}_\mathrm{b}$ for the time step $t + \Delta t$ can subsequently be determined.

In the next step of the iteration process, the load vector of the train $\mathbf{P}_\mathrm{v}$ is determined depending on the displacement u_ws and the velocity $\dot{u}_\mathrm{ws}$ of the wheel sets as well as the primary stiffness k_p and damping c_p. The equation of motion (1) of the vehicle and of the bridge are then solved separately, using the time-stepping integration method of Newmark.

For the train as well as the bridge the accelerations of the current and the previous iteration step are then compared to check the convergence criterion depending on the given tolerance

$$\frac{\|\ddot{\mathbf{U}}_n^t - \ddot{\mathbf{U}}_{n-1}^t\|}{\|\ddot{\mathbf{U}}_n^t\|} \leq \text{tolerance}. \tag{4}$$

This iterative process is repeated until the specified tolerance is reached. According to Yang and Fonder [25], the tolerance is sufficiently accurate in a range between 10^{-5} to 10^{-8} and was chosen as 10^{-5}.

5. Evaluation of interaction effects

Using the previously described MBMs of conventional and articulated trains, the additional damping occuring due to the VBI is evaluated. As a reference in the analysis of the interaction effects and the definition of the ADM, the maximum absolute accelerations at midspan obtained from the MLM and MBM computation were considered.

The procedure is presented in the following using the example of the ICE 2 [5] MBM and bridge 28 (bridge span $L = 15\,\mathrm{m}$, mass distribution $\mu = 15\,\mathrm{t/m}$, bending stiffness $EI = 11\,276\,133\,\mathrm{kNm^2}$, stiffness category $w/L = 1/2000$, modal damping ratio $\xi = 1.125\,\%$), see Figure 7.

5.1. Computational parameters

A computational time step of 0.001 s was selected for the integration of the two equations of motion (1). In case of the bridge, three eigenmodes were considered for the modal superposition principle [1].

The vehicle speed v is always assumed as constant during the bridge crossing. For the present study, the vehicle speed was varied in the range of 100 km/h to 420 km/h with a step of 1 km/h, independent of the maximum speed of the train.

5.2. Individual passage and resonance plot

The analysis was performed for all train-bridge combinations and speeds. Figure 9 presents the time histories of the acceleration of the bridge at midspan resulting from the MLM and MBM computations for one specific crossing speed for ICE 2 and bridge 28.

The interaction effect is clearly visible in form of a significant difference between the results with and without interaction. As previously mentioned, the reduction of the maximum vertical acceleration at midspan when considering interaction effects occurs due to energy transfer from the bridge to the vehicle.

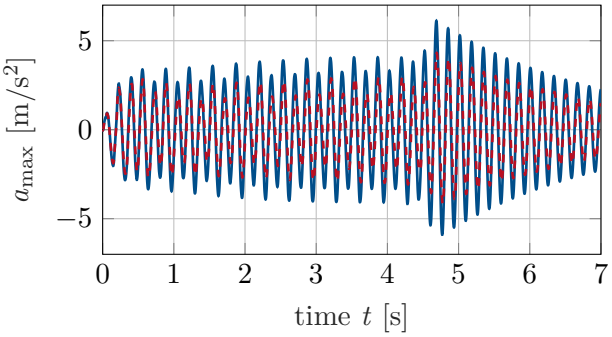


Figure 9: Acceleration at midspan $a_{\max}$ obtained from the individual passage of an ICE 2 [5] at a vehicle speed of v=284.3 km/h and bridge 28: multi-body model (- - -), moving load model (——)

From each acceleration time history, i.e. for each bridge, vehicle, and speed, the maximum absolute value is selected and represented in the resonance curve of the according train-bridge combination at the corresponding vehicle speed as shown in Figure 10.

5.3. Definition of the additional damping value

As already mentioned before, the ERRI [5] used an approach which implies a determination of the additional damping $\Delta\xi_{\mathrm{ADM}}$ by a successive increase. The additional damping is added to the modal damping ratio of the bridge in the MLM approach, until the MLM acceleration results are in close agreement with the results obtained under consideration of the VBI.

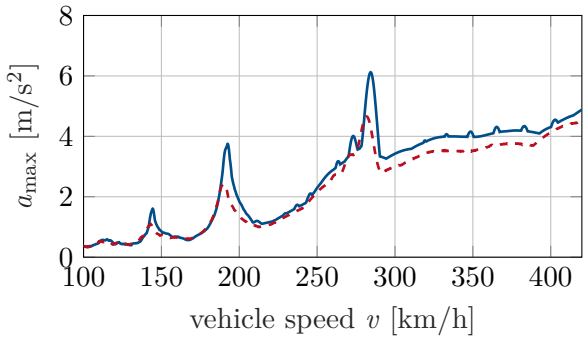


Figure 10: Max. acceleration at midspan $a_{\max}$ obtained from the passages of an ICE 2 [5] at speeds between 100 km/h to 420 km/h and bridge 28: multi-body model (- - -), moving load model (——)

This approach was also adopted for the present investigation of the additional damping value and the results from the present study are labeled as $\Delta\xi_{\text{eval}}$. Since the damping has its highest influence at resonance (see Figure 10), the corresponding crossing speed, which leads to the highest vertical acceleration at midspan of the bridge, is selected for the train-bridge combination to be investigated.

To define the additional damping $\Delta\xi_{\text{eval}}$, the resonance speed of the MLM calculation is selected by finding the peak acceleration within the resonance plot (cf. Figure 10). The resonance speed and corresponding peak acceleration of the MBM calculation is also selected and matched to the selection of the MLM. The additional damping is then evaluated by iteratively increasing the damping of the bridge in the MLM calculation until a similar maximum vertical acceleration at midspan as delivered by calculation with MBM is obtained.

In addition to a difference in peak acceleration of the resonance curve, there is also a difference in the value of the vehicle speed at which this peak level is found. This occurs due to an additional mass $\Delta\mu$ acting on the bridge during the train passage and leading to a reduction of the natural frequency of the bridge and, consequently, the resonance speed. This effect was investigated independently and is discussed in section 5.6. In what follows, this second interaction effect is not considered when computing the additional damping $\Delta\xi$, to be consistent with the procedure that was followed in [5].

5.4. Selection of the acceleration peak

As previously mentioned, the effect of the VBI is mostly pronounced in the resonant and near-resonant range (cf. Figure 10). For many train-bridge combinations like the one displayed

in Figure 10, multiple resonance peaks arise within the investigated speed range of 100 km/h to 420 km/h. The additional damping $\Delta\xi_{\text{eval}}$ is not the same for each resonance peak, so the resulting additional damping value is in fact also dependent on the considered range of vehicle speeds.

For example, if the speed range for the train-bridge combination shown in Figure 10 was limited to 250 km/h, the additional damping value would be defined by the resonance speed of about 190 km/h and results in an additional damping of $\Delta\xi_{\text{eval}} = 0.82\,\%$. A speed range up to more than 300 km/h results in an evaluation of the resonance peak at about 280 km/h and therefore an additional damping value of $\Delta\xi_{\text{eval}} = 0.74\,\%$.

In the present study, only the highest peak is selected for the evaluation of the additional damping $\Delta\xi_{\text{eval}}$, but this means that considering another range of crossing speeds (i.e. another upper speed limit), might lead to another resonance peak being decisive for the given train-bridge combination.

The ERRI [5] considered a range of vehicle speeds between 180 km/h and 350 km/h while the present study considers a range of vehicle speeds between 100 km/h and 420 km/h, as previously mentioned.

5.5. Influence of 3-point load distribution

For reproduction and comparison of the results presented in this study, it is important to note how the loads of the train were distributed. This subsection illustrates how the assumed load distribution affects the results reported in in this study. A closer investigation of the bridge acceleration ratio between distributed loads and point loads was performed by Jin et al. [26].

A 3-point load distribution of the axle loads in longitudinal direction according to EC 1 [3] was used in the present investigations, although it is not clear if this was also used in [5]. It implies the distribution of each axle load on three neighbouring sleepers lying 0.65 m apart from each other. Half of the axle load is assigned to the middle sleeper, while a quarter of the load is applied to each of the neighbouring sleepers. This does not influence the coupling points of bridge and train as described in section 4.1, where only the actual axle position is used.

As shown in Figure 11, the longitudinal distribution of the axle loads leads to a decrease of the maximum accelerations of the resonance curves both in case of the MLM and MBM computations. Moreover, it also has an influence on the calculated additional damping $\Delta\xi$, as indicated in Figure 11. In the following, the load distribution was defined based on a sleeper spacing of 65 cm, as

defined in the German national annex of EC 1 [3]. The resulting curve of the MLM with a load distribution of 65 cm and $\Delta\xi$ is also presented in Figure 11.

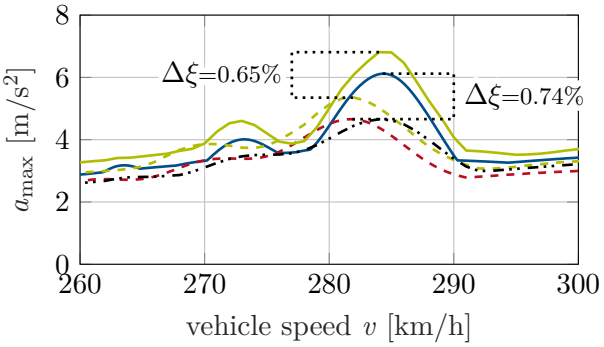


Figure 11: Max. acceleration at midspan $a_{\max}$ obtained from the passages of an ICE 2 [5] at speeds between 260 km/h to 300 km/h and bridge 28: multi-body model (MBM) without load distribution (- - -), moving load model (MLM) without load distribution (——), MBM with load distribution 65 cm (- - -), MLM with load distribution 65 cm (——), MLM with load distribution 65 cm and $\Delta\xi = 0.74\%$ (-··-)

5.6. Influence of additional mass, resonance shift

As it can be observed from Figure 10, the consideration of VBI also leads to a horizontal shift of the resonance peaks. It is presumed that this shift occurs mainly due to the unsprung mass of the train itself [24, 28, 32].

The increasing of the bridge mass distribution μ by a component $\Delta\mu$ seems therefore a justifiable approach, which allows the reproduction of the resonance speed drop using the MLM approach and will be investigated in more detail in what follows.

According to the Austrian guidelines from 2007 [33], an additional mass of 2 t/m (corresponding to a load of 20 kN/m and thus also approximately the mean value of all train masses of the HSLM-A load diagrams) is to be added to the structure mass in order to account for the possible frequency drop of the bridge occurring due to the additional train mass. However, as mentioned before, it is expected that the car body is dynamically uncoupled from the bridge, so it seems unlikely that the whole train mass needs to be added to the bridge mass. This might explain why the specification has been eliminated from the newly released Austrian guideline for Dynamic computation of Railway bridges [34].

In a similar way as the additional damping values $\Delta\xi$ were determined, an iterative approach was followed to evaluate the additional mass $\Delta\mu$ and adjust the horizontal shift of the resonance

peak. By iteratively increasing the bridge mass for the MLM calculation, the resonance speed is reduced and matched to the interaction result, disregarding the reduced maximum acceleration at midspan for the interaction result. An accurate determination of the additional mass required a reduction of the speed increment from 1 km/h to 0.1 km/h.

For example, the results shown in Figure 12 indicate a reduction of the resonance speed from 284.3 km/h to 281.8 km/h. This corresponds to an additional mass $\Delta\mu$ of 280.7 kg/m.

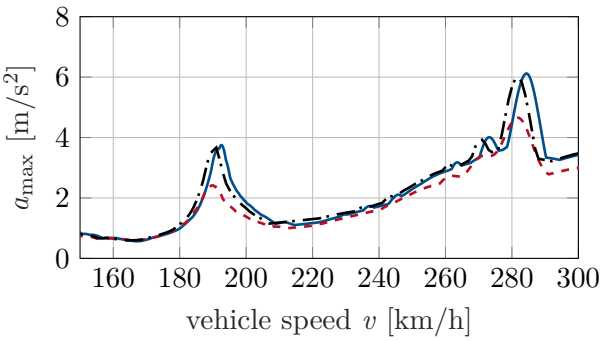


Figure 12: Max. acceleration at midspan $a_{\max}$ obtained from the passages of an ICE 2 [5] at speeds between 150 km/h to 300 km/h and bridge 28: multi-body model (- - -), moving load model (——), moving load model with additional mass $\Delta\mu = 280.7$ kg/m (—·—)

5.7. Investigation of additional mass for a larger data set

The previously presented method for determination of the additional mass $\Delta\mu$ was subsequently applied to further bridges considered in the data set of this paper.

The results are shown in Figure 13 and indicate an additional mass between 224 kg/m and 428.2 kg/m. This leads to the presumption that the additional mass corresponds approximately to the mass of the wheel sets distributed over the train length of the ICE 2 ($\mu_{\text{ws}} = 290$ kg/m).

To investigate this trend, the additional mass $\Delta\mu$ was compared to the mass of the wheel sets distributed across the train length for all investigated trains and three selected bridges. Figure 14 shows that all additional masses $\Delta\mu$ lie in the same range around 200 kg/m to 400 kg/m which equals the mass of the wheel sets distributed across the train length. This finding can be explained by the uncoupling of the car body masses from the bridge, which occurs when the natural frequency of the car body modes (bouncing mode about 1 Hz, see Figure 6a) is sufficiently lower than the natural frequency of the relevant vertical bending mode of the bridge (usually > 5 Hz). In this case, the unsprung mass of the wheel sets is directly connected to the bridge while the car body masses

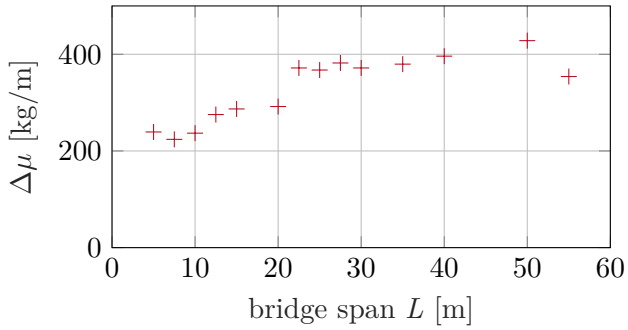


Figure 13: Additional mass $\Delta\mu$ depending on bridge span L of different bridges and ICE 2 [5]

are dynamically isolated from the bridge through the suspension system at frequencies above the bouncing mode of the car body. The vertical bouncing modes of the bogies cover a wide range (see Figure 6a). Therefore, the bogies are dynamically coupled to the bridges in some combinations of trains and bridges, explaining the scatter in results of the additional mass.

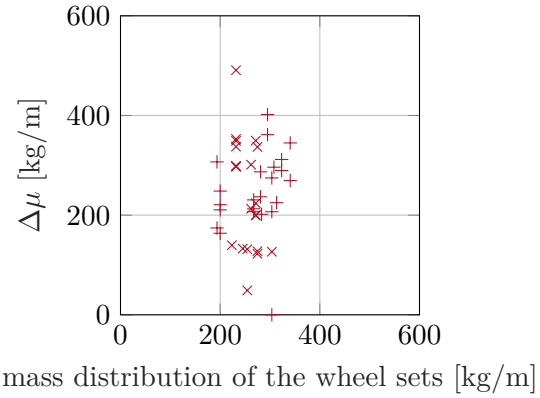


Figure 14: Additional mass $\Delta\mu$ depending on the mass distribution of the wheel sets across train length μ_{ws} for bridges 16, 28 and 40: articulated (×) and conventional (+) trains

In the following sections of this paper, the results will be evaluated only regarding the reduction of the maximum acceleration to define the additional damping $\Delta\xi_{\mathrm{eval}}$ as it was also investigated by the ERRI [5].

6. Analysis of the additional damping when determined as a tuning parameter based on the moving loads and the multi-body model

A total number of more than 800 000 crossings was calculated with and without interaction for the complete data sets of 25 trains and over 100 bridges, described in sections 2 and 3. In the following, the results are first used to represent the additional damping value as a function of the bridge span L, similar to the original investigation of [5] concerning the determination of the ADM included in EC 1 [3] and RIL 804 [4]. Even though the ADM is only applicable to bridge spans up to 30 m, the bridge set was extended up to spans of 55 m, to verify the findings by Arvidsson and Karoumi [6] concerning the coupling effects for long bridges.

6.1. Comparison of calculations to ERRI

The bridges that were considered by the ERRI [5] for the definition of the ADM are comprised in set A in Figure 8. Figure 15 shows the comparison between the ADM curve from EC 1 [3] and the results obtained for bridge set A and the two vehicles considered in [5] (Eurostar and ICE 2). It indicates that the evaluation of the additional damping according to the method described in section 5 mostly results in additional damping values lying above the curve provided in [3], confirming thus the conservative character of the ADM for these specific cases (see Figure 15). Differences in the results are due to the simplified interaction model used by the ERRI [5] and the detailed MBM used in the present study.

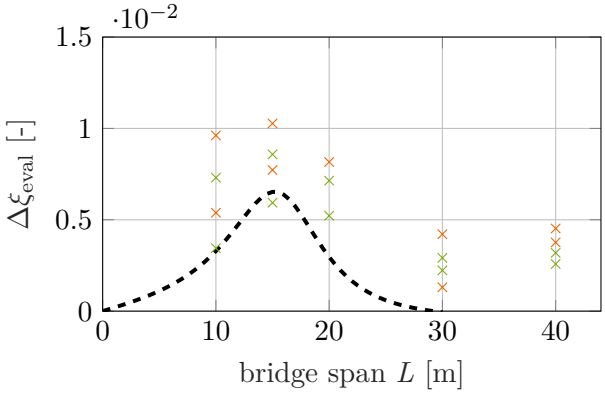


Figure 15: $\Delta\xi_{\text{ADM}}$ [3] (- - -) compared to $\Delta\xi_{\text{eval}}$ of Eurostar (×) and ICE 2 (×) for bridge set A

It is to be mentioned, that no additional damping was evaluated for ICE 2 and bridge number 6 (bridge span $L = 20$ m), since no resonance peak was identified in the speed range between 180 km/h

to 350 km/h, which was considered by the ERRI [5] (see Figure 16).

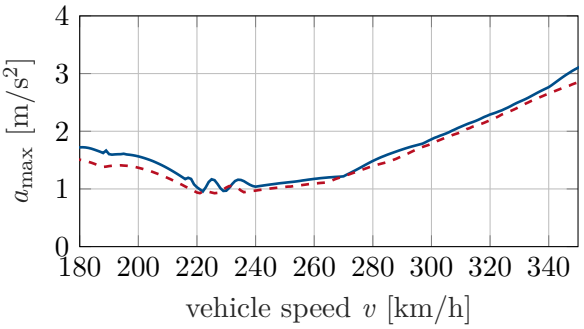


Figure 16: Max. acceleration at midspan $a_{\max}$ obtained from the passages of an ICE 2 [5] at speeds between 180 km/h to 350 km/h and bridge 6 ($L = 20$ m, $\mu = 15$ t/m, $EI = 24\,461\,700$ kNm^2, $w/L = 1/2000$, $\xi = 1\,\%$): multi-body model (- - -), moving load model (——)

Nevertheless, if the analysis of the interaction effects is extended to all 100 bridges, still considering the same two trains, there are multiple additional damping values that undercut the curve provided in EC 1 [3] (see Figure 17). This confirms the unconservative character of the ADM reported in previous research.

6.2. Evaluation of all results based on bridge span

The results of the additional damping $\Delta\xi_{\text{eval}}$ obtained for all 25 trains and 100 bridges are illustrated in Figure 18. The plot clearly shows that the ADM curve specified in EC 1 [3] and RIL 804 [4] overestimates the actual values of the additional damping in many cases. Therefore, it can be stated that the small set of train-bridge combinations as used by the ERRI [5] and presented in Figure 15 is too narrow and not representative for a reliable determination of the additional damping.

Although the median of all results from the data set seems to comply with the ADM curve, adopting $\Delta\xi_{\text{ADM}}$ in design calculations leads to an overestimation of the actual interaction effect in several cases. The right way to define the additional damping would be to choose the minimal values to avoid an overestimation. As shown in Figure 18, the lowest values prohibit the definition of conservative additional damping values, which can be safely adopted in design.

Still, for all bridge spans there are train-bridge combinations leading to additional damping values above 0.5 % indicating a significant interaction effect. Therefore, as already noted by Arvidsson

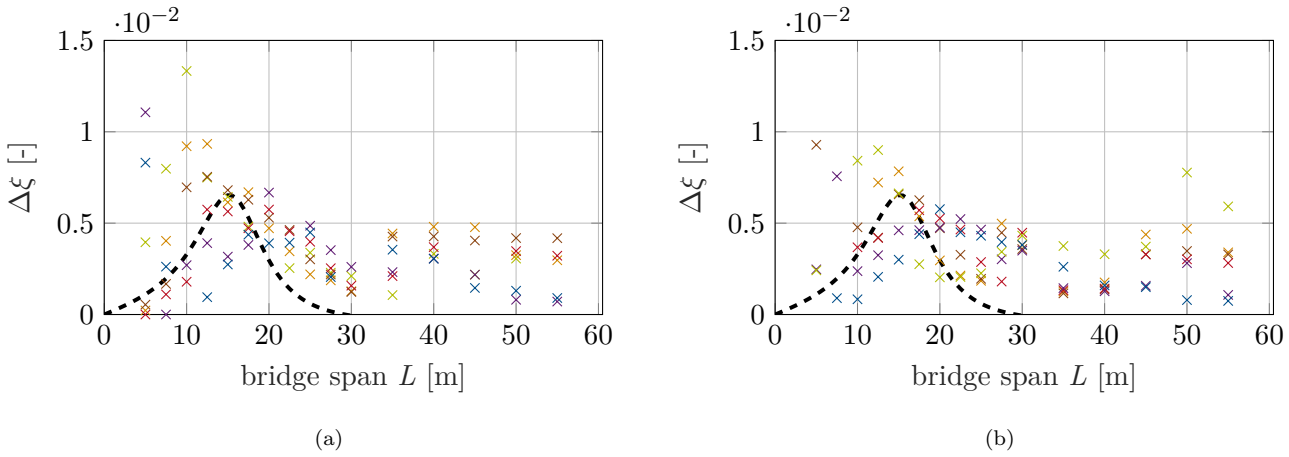


Figure 17: $\Delta\xi_{\mathrm{ADM}}$ [3] (- - -) compared to $\Delta\xi_{\mathrm{eval}}$ of Eurostar and ICE 2 (stiffness categories w/L: × 1/600, × 1/1000, × 1/1500, × 1/2000, × 1/3000, × 1/5000): (a) ICE 2, (b) Eurostar

and Karoumi [6], it can be said that coupling effects can also be significant for long bridges with spans over 30 m.

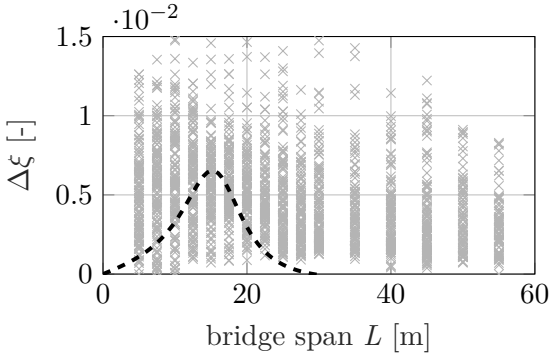


Figure 18: $\Delta\xi_{\mathrm{ADM}}$ [3] (- - -) compared to $\Delta\xi_{\mathrm{eval}}$ for all train-bridge combinations (20 values above 1.5 % were found)

Furthermore, the results in Figure 18 do not show a clear trend of the additional damping in terms of the bridge span L as proposed by [5]. This was already concluded in previous research works (e.g. [2]). Therefore, it is worth investigating if a more clear correlation of the additional damping with respect to other parameters can be identified to incorporate the VBI effects in MLM calculations, as also suggested by other researchers.

6.3. Additional damping dependent on ratios of length, frequency and mass

According to Doménech et al. [2], the additional damping depends on the bridge-to-vehicle ratios of length, frequency and mass. The investigation by Doménech et al. [2] was based on train

models of the ICE 2 and the ETR 500Y. Therefore, the results of the present study for these two trains are presented in Figure 19 to investigate the trends given in [2].

The length ratio is defined as the ratio between the bridge span L and the car body length D:

$$\beta_{\mathrm{D}} = \frac{L}{D} \tag{5}$$

Doménech et al. [2] indicate an increase of the additional damping value with the length ratio β_{D} for fixed values of the frequency ratio η_{bouncing}. This statement cannot be confirmed by the present study (see Figure 19a), as the low additional damping values for β_{D} below 1 show a wide scatter. This can be explained by the low mass ratio γ_{b} of these train-bridge combinations, since the shorter bridges in the bridge set also have a lower mass, which influences the mass ratio γ_{b}.

The mass ratio γ_{b} represents the ratio between the bridge mass and the average bogie mass:

$$\gamma_{\mathrm{b}} = \frac{m_{\mathrm{bridge}}}{m_{\mathrm{b}}} \tag{6}$$

Figure 19b shows the additional damping value as a function of γ_{b}. Doménech et al. [2] found a decrease of the additional damping with the mass ratio γ_{b} for fixed values of the frequency ratio η_{bouncing}. As the length ratio also varies within the investigated train-bridge combinations, this trend cannot be confirmed independently of the length ratio β_{D}.

The frequency ratio is defined as:

$$\eta_{\mathrm{bouncing}} = \frac{n_0}{n_{\mathrm{bouncing,bogie}}} \tag{7}$$

Furthermore, according to Doménech et al. [2], the additional damping is reaching higher values when η_{bouncing} (ratio between the bridge fundamental frequency and the bogie vertical frequency) approaches unity. The results presented in Figure 19c show, that the peak is slightly off unity. It is presumed that this is due to the interaction effect of train and bridge, which is similar to what is observed in the interaction of a tuned mass damper and the main structure [1, 35]. The frequency ratio η_{bouncing} was also examined more closely by Jin et al. [22], who found the peak value to be also dependent on β_{D}.

The analysis was done for the complete set of trains and bridges. Also 3D plots of two ratios defined by Doménech et al. [2] were checked to investigate the joint dependency on two parameters but without any conclusive analysis.

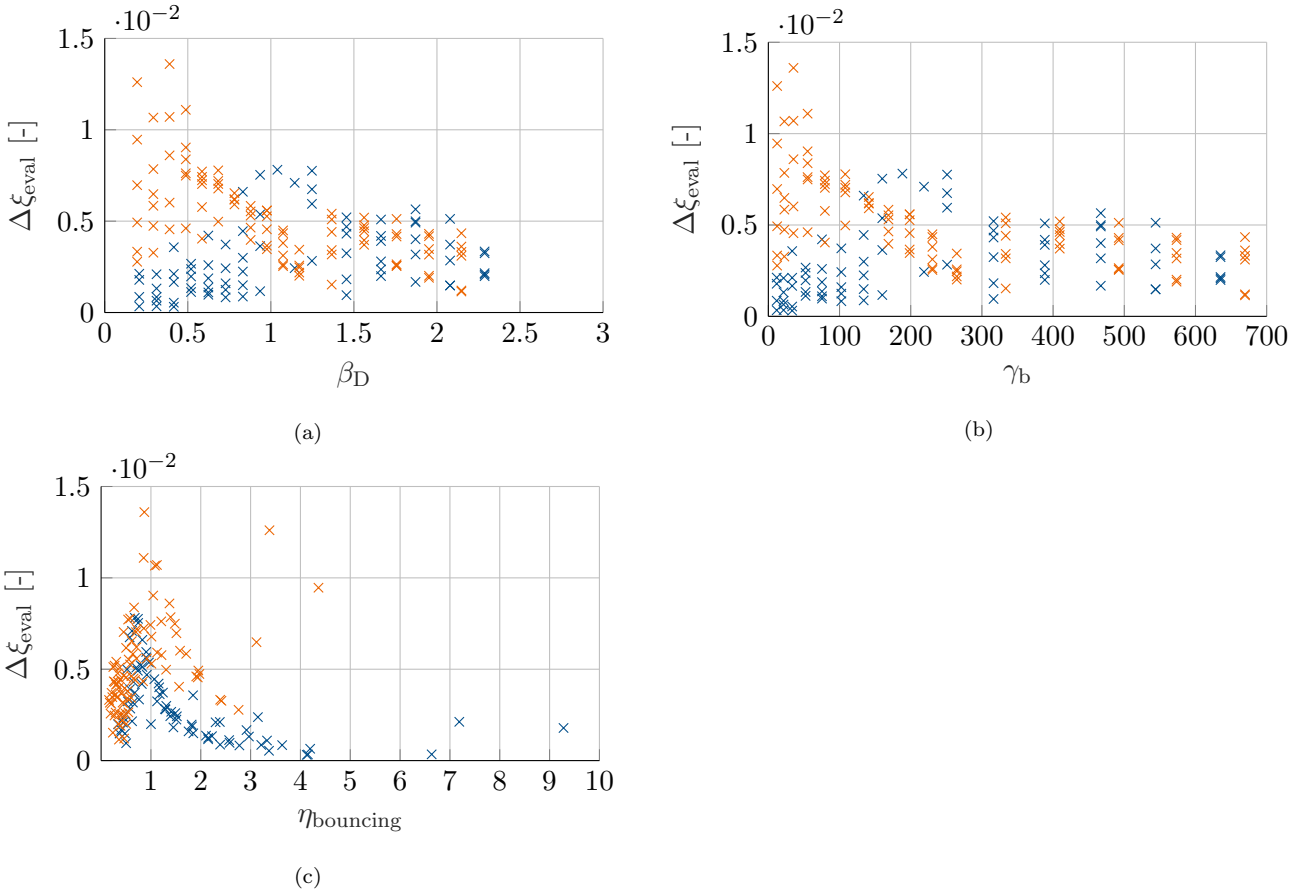


Figure 19: $\Delta\xi_{\text{eval}}$ of ICE 2 (×) and ETR 500Y (×) as a function of the parameter ratios defined by Doménech et al. [2]: (a) β_{D}, (b) γ_{b}, (c) η_{bouncing}

7. Analysis of the additional damping as a function of mechanical parameters based on simplified coupled models

In this section, the results obtained for the comprehensive set of train-bridge combinations are used to study the approaches by Yau et al. [7] and Stoura and Dimitrakopoulos [8], where values of the additional damping are derived based on simplified mechanical models. Firstly, the approaches are described to explain how the additional damping values can be derived from the MBM characteristics of the data set. Next, the train-bridge combination considered in the previous example (ICE 2 and bridge 28) is used to visualize the results for the additional damping values according to [7] and [8].

Since both approaches evaluate the characteristics of one carriage of the train, they imply a conventional and (close to) homogeneous train, which is in fact only the case for a small subset of

the database considered in this work. The approaches were therefore applied to the passenger cars of seven conventional trains from the data set, that can be considered as close to homogeneous. The traction cars of the trains were also investigated, but the investigations lead to better results for the passenger cars in most cases, which seems reasonable, since these make up the main part of the trains (e.g. ICE 2 used by ERRI [5] has 12 identical passenger cars and two traction cars). Therefore, only results of the passenger cars will be discussed in the following.

It is to be mentioned that the approaches from Yau et al. [7] and Stoura and Dimitrakopoulos [8] were not applied in relation to articulated trains. The reason for this is that the approach proposed for the additional damping is based on a single, independent carriage as found in conventional trains and cannot be straightforwardly applied to an articulated train, since the carriages have a vertical connection (see section 2.3).

7.1. Equivalent Additional Damping Approach

Yau et al. [7] developed an alternative analytical approach for simply supported bridges and (close to) homogeneous conventional trains, namely the Equivalent Additional Damping Approach (EADA). The approach considers the vehicle's dynamic characteristics when estimating the additional damping on a bridge due to VBI to predict the peak response at resonance. It uses a simplified model for conventional carriages, which simulates one carriage as two equivalent identical single-DOF oscillators. The modal mass m_1 and stiffness k_1 of the vehicle are obtained from an eigenvalue analysis of one individual conventional carriage as

$$m_1 = \frac{1}{2}\varphi_1^{\mathrm{T}}\mathbf{M}_{\mathrm{v}}\varphi_1, \qquad k_1 = \frac{1}{2}\varphi_1^{\mathrm{T}}\mathbf{K}_{\mathrm{v}}\varphi_1 \tag{8}$$

with the first vertical mode of the car body φ_1 and the mass and stiffness matrix of the vehicle ($\mathbf{M}_{\mathrm{v}}$ and $\mathbf{K}_{\mathrm{v}}$).

The single-span bridge is also modeled as a single-DOF oscillator with the modal mass M_1, modal stiffness K_1, and modal damping C_1.

The equivalent parameters γ_1, η_1, and $\xi_{\mathrm{v}1}$ were identified as the vehicle parameters governing the interaction effects [7]. The modal mass ratio (tuning unit in reducing the vibration of the bridge mass) is defined as:

$$\gamma_1 = \frac{m_1}{M_1}. \tag{9}$$

The frequency ratio of the coach-bridge system η_1 is the ratio between the car body vertical frequency $n_{\text{bouncing, car body}}$ and the bridge fundamental frequency n_0:

$$\eta_1 = \frac{n_{\text{bouncing, car body}}}{n_0}. \tag{10}$$

The effective suspension damping ratio ξ_{v1} is defined as:

$$\xi_{\text{v1}} = \frac{c_1}{2m_1\omega_{\text{v1}}} \qquad \text{with} \qquad \omega_{\text{v1}} = \sqrt{\frac{k_1}{m_1}}. \tag{11}$$

The additional damping $\Delta\xi_{\text{EADA}}$ is calculated from the given equivalent parameters and added to the modal damping of the bridge C_1:

$$\Delta\xi_{\text{EADA}} = \gamma_1\eta_1\left|\frac{\eta_1 + 2\xi_{\text{v1}}\text{i}}{(1-\eta_1^2) - 2\xi_{\text{v1}}\eta_1\text{i}}\right|. \tag{12}$$

Equation (12) can be simplified as:

$$\Delta\xi_{\text{EADA}} = \gamma_1\eta_1\sqrt{\eta_1^2 + (2\xi_{\text{v1}})^2} \tag{13}$$

with the approximation of $|(1-\eta_1^2) - 2\xi_{\text{v1}}\eta_1\text{i}| \simeq 1$ for the vertical frequency ratio η_1 (see equation 10) of a short bridge being considerably less than unity based on the strict requirements of riding comfort for high speed trains [7].

7.2. Additional damping based on the impedance ratio

In [8], Stoura and Dimitrakopoulos investigated the interaction effect of high-speed trains with simply supported and continuous bridges. Their work aims for a systematic approach for several train-bridge combinations. Their approach for an equivalent additional damping ratio for simply supported bridges is based on the impedance ratio and defined as:

$$\Delta\xi_{\text{imp}} = \frac{C_{\text{i}}}{2}\left(\frac{L}{r_{\text{mode}}\, d_{\text{av}}} + \frac{1}{2}\right). \tag{14}$$

Where C_{i} (see equation 15) is the impedance ratio, d_{av} is the average distance between adjacent wheels (4.7 m to 6.5 m according to [8]), and r_{mode} is the mode number (chosen as 1 for the comparisons performed in the present study). The impedance ratio is expressed as:

$$C_{\text{i}} = \Sigma c_{\text{p}}/(2M_1 n_0) \tag{15}$$

with the sum of primary damping of one carriage Σc_p, the generalized mass of the bridge M_1, and the eigenfrequency of the fundamental mode of the bridge n_0. The mechanical impedance $M_1 n_0$ denotes the bridge's inertial resistance to free vibrations [8].

Substituting the introduced parameters, equation 14 becomes:

$$\Delta\xi_\mathrm{imp} = \Sigma c_\mathrm{p} \frac{L}{(r_\mathrm{mode}\pi)^2\sqrt{EI\mu)}} \left(\frac{L}{r_\mathrm{mode} d_\mathrm{av.}} + \frac{1}{2} \right). \tag{16}$$

According to Stoura and Dimitrakopoulos [8], the additional damping value increases for longer spans and for higher values of the impedance ratio C_i.

7.3. Comparison of the results with literature approaches

Figure 20 shows the comparison of the interaction results for one exemplary train-bridge combination to the results with a MLM. The latter one is considered in three variations: without additional damping and with additional damping $\Delta\xi_\mathrm{EADA}$ according to [7] and $\Delta\xi_\mathrm{imp}$ according to [8]).

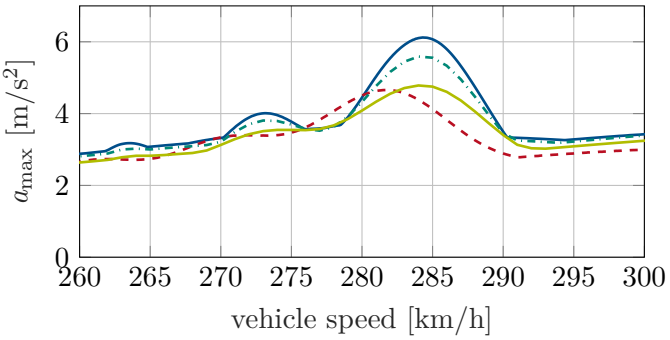


Figure 20: Max. acceleration at midspan a_max obtained from the passages of an ICE 2 [5] at speeds between 260 km/h to 300 km/h and bridge 28: multi-body model (- - -), moving load model without additional damping (——), MLM with $\Delta\xi_\mathrm{EADA}$ according to [7] (-·-·-), MLM with $\Delta\xi_\mathrm{imp}$ according to [8] (——)

As $\Delta\xi_\mathrm{eval}$ equals 0.74 % for this specific train-bridge combination, the additional damping result for the passenger cars of the ICE 2 according to [7] (0.20 %) seems to underestimate the interaction effect. A slight underestimation is also revealed by the approach of [8] (0.65 %), see Figure 20.

To display the results for multiple bridges, the relative deviation of the additional damping according to [7] ($\Delta\xi_\mathrm{EADA}$) and [8] ($\Delta\xi_\mathrm{imp}$) with respect to the additional damping $\Delta\xi_\mathrm{eval}$ from this

study is defined as:

$$\text{relative deviation} = \frac{\Delta\xi_{\text{comparison}} - \Delta\xi_{\text{eval}}}{\Delta\xi_{\text{eval}}} \tag{17}$$

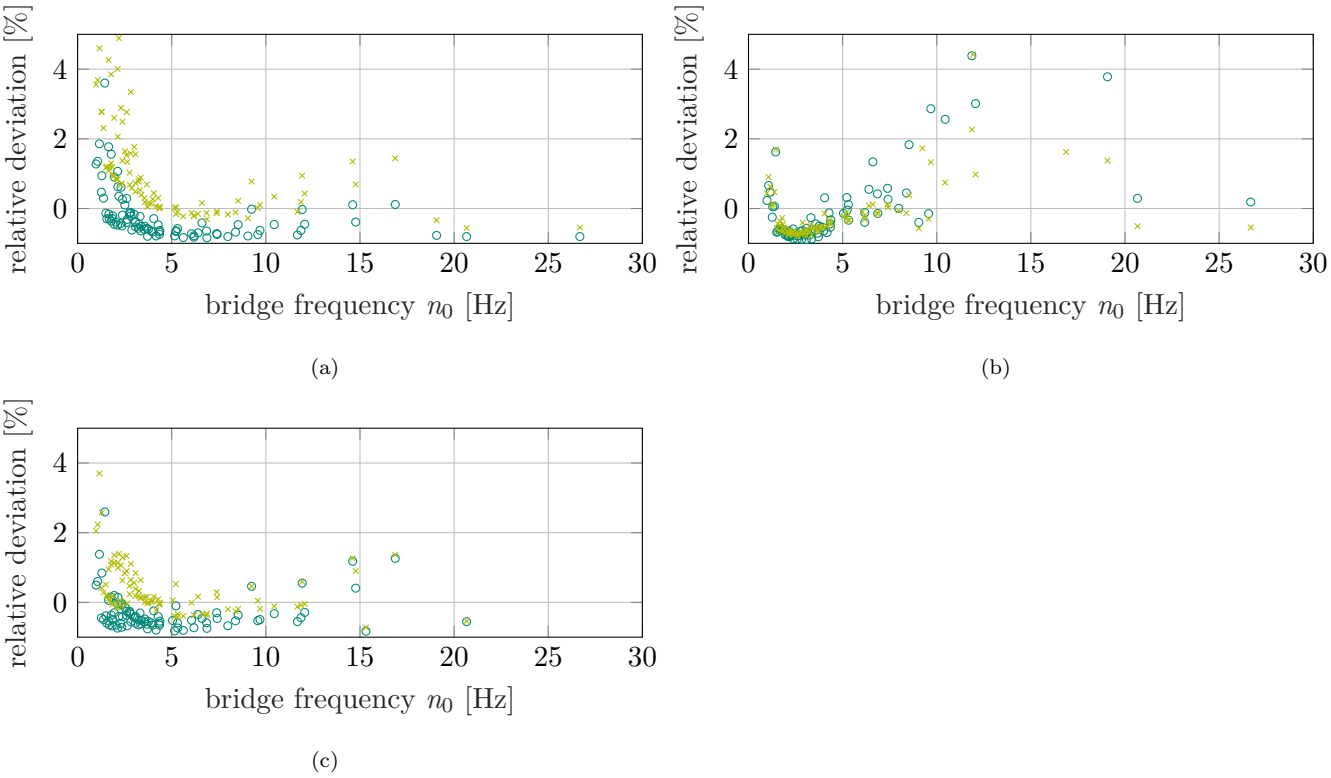


Figure 21: Relative deviation of the approaches of Yau et al. [7] (○) resp. Stoura and Dimitrakopoulos [8] (×) for passenger cars with respect to the additional damping $\Delta\xi_{\text{eval}}$: (a) ICE 2 from ERRI [5], 1 value exceeding 5 % for Stoura; (b) ETR500Y, 3 values exceeding 5 % for Yau; (c) Railjet, 1 value exceeding 5 % for Stoura

The relative deviation is plotted in terms of different bridge frequencies n_0 in Figure 21. It can be seen that the error mostly lies below 5 %, indicating good results of both approaches for the passenger cars of the almost homogeneous trains ICE 2, ETR500Y, and Railjet.

It is noticeable, that the additional damping is overestimated by both approaches for bridges with very low eigenfrequencies (between 0 Hz to 1 Hz). Presumably, this effect occurs due to the very low difference between the bridge and the car body frequency (ICE 2 ERRI: 0.64 Hz, ETR500Y: 0.35 Hz, Railjet: 0.53 Hz). This leads most likely to a dynamic coupling between the bridge and the car body.

It can be generally stated that both approaches succeed in defining additional damping values that capture the relevant interaction effects well, but at the expense of requiring the values of

the train characteristics appearing in the expressions. Although the train characteristics for some MBMs are found in literature, as collected in the presently used train data set, it is not clear whether these correctly represent the real train behaviour and they are by far not available for all trains. It can be concluded that detailed information about the train characteristics is needed in order to achieve a more reliable result for the additional damping. Therefore, this information needs to be made available by train manufacturers but may also require them to comply with certain ranges for all future trains to be brought in operation.

8. Conclusion

In this work, the additional damping was studied by analyzing a comprehensive set of trains and bridges. The additional damping was defined by means of an iterative process, implying the iterative adaptation of the structural damping in case of a moving load computation until the maximum acceleration at midspan matches the results of a multi-body model computation, i.e. under full consideration of the interaction effects.

The set of characteristics for 25 multi-body vehicle models was used for an investigation of the parameter ranges. The comprehensive computational series with these vehicles revealed multiple cases with very low additional damping values. This confirms earlier findings by Doménech et al. [2], performed on a smaller set of trains and bridges. The results also showed that it was not possible to define a conservative value of the additional damping by considering the bridge span only, as assumed by Eurocode 1 [3] and RIL 804 [4].

A more reliable characterization of the additional damping requires taking into account more information on the train and bridge characteristics, as indicated in the works of Yau et al. [7] and Stoura and Dimitrakopoulos [8]. This is in line with the main conclusion of the present study, which states that an adequate characterization of the additional damping requires knowledge of the dynamic characteristics of the vehicle and the bridge. This means that the improved accuracy of the additional damping models occurs at the expense of requiring more detailed knowledge of the train characteristics, which is currently not publicly available for all operating trains, thus hindering the direct implementation of these approaches in practice. It was shown that the methods by [7] and [8] generally lead to values of the additional damping that capture the interaction effects well when used in combination with a moving load model. However, it is to be noted that the approaches by

[7] and [8] are at present only applicable to near to homogeneous conventional trains, still requiring an extension to more heterogeneous or articulated trains. If these approaches would be adopted for the practical application, a commitment for the vehicle manufacturers would be required. On the one side, they would have to make the information about their train characteristics publicly available and on the other side, they might have to comply to certain parameter ranges for future developments.

9. Acknowlegments

The work on which this report is based was carried out on behalf of the Federal Minister of Transport and Digital Infrastructure (FE-Nr. 2019-T-1-1217). Responsibility for the content lies solely with the authors. The authors would like to thank the members of the steering committee: EBA, DB Netz AG and ÖBB-Infrastruktur AG and the working group Vehicle and Bridge Dynamics for the excellent cooperation and the valuable technical discussions.

References

[1] C. Petersen, Dynamik der Baukonstruktionen, 2017. doi:10.1007/978-3-322-80314-6.

[2] A. Doménech, P. Museros, M. D. Martínez-Rodrigo, Influence of the vehicle model on the prediction of the maximum bending response of simply-supported bridges under high-speed railway traffic, Engineering Structures 72 (2014) 123–139. doi:10.1016/j.engstruct.2014.04.037.

[3] EN 1991-2 ANB:2011-10 (2011): Eurocode 1 : Actions on structures - Part 2 : Traffic loads on bridges - National annex (2011).

[4] DB Netz AG, Richtlinie 804: Eisenbahnbrücken (und sonstige Ingenieurbauwerke) planen, bauen und instand halten (2013).

[5] ERRI-Sachverständigenausschuss D 214, RP 4:1999-12: Wechselwirkung zwischen Zug und Brücke, Tech. rep., Europaisches Institut für Eisenbahnforschung (ERRI), Utrecht (1999).

[6] T. Arvidsson, R. Karoumi, Train–bridge interaction – a review and discussion of key model parameters, International Journal of Rail Transportation 2 (3) (2014) 147–186. doi:10.1080/23248378.2014.897790.
URL http://dx.doi.org/10.1080/23248378.2014.897790

[7] J. D. Yau, M. D. Martínez-Rodrigo, A. Doménech, An equivalent additional damping approach to assess vehicle-bridge interaction for train-induced vibration of short-span railway bridges, Engineering Structures 188 (January) (2019) 469–479. doi:10.1016/j.engstruct.2019.01.144.
URL https://doi.org/10.1016/j.engstruct.2019.01.144

[8] C. D. Stoura, E. G. Dimitrakopoulos, Additional damping effect on bridges because of vehicle-bridge interaction, Journal of Sound and Vibration 476 (2020) 1–16. doi:10.1016/j.jsv.2020.115294.

[9] K. Liu, E. Reynders, G. De Roeck, G. Lombaert, Experimental and numerical analysis of a composite bridge for high-speed trains, Journal of Sound and Vibration 320 (1-2) (2009) 201–220. doi:10.1016/j.jsv.2008.07.010.

[10] A. M. Kohl, K.-D. Clement, Data sets of multi-body models for conventional and articulated trains and single span bridges, Tech. rep., Institute for Structural Mechanics and Design, TU Darmstadt (2022). doi:10.5281/zenodo.6696665.

[11] P. A. Costa, R. Calçada, A. S. Cardoso, Influence of train dynamic modelling strategy on the prediction of track-ground vibrations induced by railway traffic, Proceedings of the Institution of Mechanical Engineers, Part F: Journal of Rail and Rapid Transit 226 (4) (2012) 434–450. doi:10.1177/0954409711433686.

[12] K. Liu, G. De Roeck, G. Lombaert, The effect of dynamic train-bridge interaction on the bridge response during a train passage, Journal of Sound and Vibration 325 (1-2) (2009) 240–251. doi:10.1016/j.jsv.2009.03.021.

[13] E. Andersson, O. Fröidh, S. Stichel, T. Bustad, H. Tengstrand, Green Train: concept and technology overview, International Journal of Rail Transportation 2 (1) (2014) 2–16. doi:10.1080/23248378.2013.878291.

[14] N. Zhang, H. Xia, W. Guo, Vehicle-bridge interaction analysis under high-speed trains, Journal of Sound and Vibration 309 (3-5) (2008) 407–425. doi:10.1016/j.jsv.2007.07.064.

[15] B. Glatz, J. Fink, Einfluss der Zugmodelle auf die dynamische Antwort von 75 Stahl-, Verbund- und Stahlbeton-brücken, Stahlbau 88 (5) (2019) 470–477. doi:10.1002/stab.201900014.

[16] A. Firus, H. Berthold, J. Schneider, G. Grunert, Untersuchungen zum dynamischen Verhalten einer Eisenbahnbrücke bei Anregung durch den neuen ICE4, in: VDI Berichte 2321, VDI-Fachtagung Baudynamik, Würzburg, Deutschland, 2018, pp. 233–248.

[17] P. Galvín, A. Romero, J. Domínguez, Fully three-dimensional analysis of high-speed traintracksoil-structure dynamic interaction, Journal of Sound and Vibration 329 (24) (2010) 5147–5163. doi:10.1016/j.jsv.2010.06.016.

[18] G. Kouroussis, O. Verlinden, C. Conti, Free field vibrations caused by high-speed lines: Measurement and time domain simulation, Soil Dynamics and Earthquake Engineering 31 (4) (2011) 692–707. doi:10.1016/j.soildyn.2010.11.012.

[19] Y. S. Lee, S. H. Kim, Structural analysis of 3D high-speed train-bridge interactions for simple train load models, Vehicle System Dynamics 48 (2) (2010) 263–281. doi:10.1080/00423110902751912.

[20] P. Galvín, S. François, M. Schevenels, E. Bongini, G. Degrande, G. Lombaert, A 2.5D coupled FE-BE model for the prediction of railway induced vibrations, Soil Dynamics and Earthquake Engineering 30 (12) (2010) 1500–1512. doi:10.1016/j.soildyn.2010.07.001.

[21] B. Glatz, J. Fink, A redesigned approach to the additional damping method in the dynamic analysis of simply supported railway bridges, Engineering Structures 241 (March) (2021) 112415. doi:10.1016/j.engstruct.2021.112415.

URL https://doi.org/10.1016/j.engstruct.2021.112415

[22] Z. Jin, B. Huang, S. Pei, Y. Zhang, Energy-based additional damping on bridges to account for vehicle-bridge interaction., Engineering Structures 229 (2021).

[23] K. Matsuoka, K. Kaito, M. Sogabe, Bayesian time–frequency analysis of the vehicle–bridge dynamic interaction effect on simple-supported resonant railway bridges, Mechanical Systems and Signal Processing 135 (2020)

106373. doi:10.1016/j.ymssp.2019.106373.
URL https://doi.org/10.1016/j.ymssp.2019.106373

[24] T. C. Mähr, Theoretische und experimentelle Untersuchungen zum dynamischen Verhalten von Eisenbahnbrücken mit Schotteroberbau unter Verkehrslast (2008).

[25] F. Yang, G. A. Fonder, An iterative solution method for dynamic response of bridge-vehicles systems, Earthquake Engineering and Structural Dynamics 25 (2) (1996) 195–215. doi:10.1002/(SICI)1096-9845(199602)25:2<195::AID-EQE547>3.0.CO;2-R.

[26] Z. Jin, B. Huang, J. Ren, S. Pei, Reduction of vehicle-induced vibration of railway bridges due to distribution of axle loads through track, Shock and Vibration 2018 (1) (2018). doi:10.1155/2018/2431980.

[27] K. Liu, N. Zhang, H. Xia, G. De Roeck, A comparison of different solution algorithms for the numerical analysis of vehicle-bridge interaction, International Journal of Structural Stability and Dynamics 14 (2) (2014) 1–17. doi:10.1142/S021945541350065X.

[28] J. Li, M. Su, L. Fan, Natural Frequency of Railway Girder Bridges under Vehicle Loads 8 (4) (2003) 199–203. doi:10.1061/(ASCE)1084-0702(2003)8.

[29] S. H. C. Toit du, Graphical exploratory data analysis, Springer, 2012.

[30] F. E. Grubbs, Procedures for Detecting Outlying Observations in Samples, Technometrics 11 (1969). doi:10.1080/00401706.1969.10490657.

[31] K. Liu, Analysis and Monitoring of Dynamic Effects of Train-Bridge Interaction, 2010.

[32] K. Liu, G. Lombaert, G. De Roeck, Dynamic Analysis of Multispan Viaducts with Weak Coupling between Adjacent Spans, Journal of Bridge Engineering 19 (1) (2014) 83–90. doi:10.1061/(asce)be.1943-5592.0000476.

[33] ÖBB, Richtlinie für die dynamische Messung von Eisenbahnbrücken (2007).

[34] ÖBB, Richtlinie für die dynamische Messung von Eisenbahnbrücken (2022).

[35] Y. Fujino, M. Abé, Design formulas for tuned mass dampers based on A perturbation technique, Earthquake Engineering & Structural Dynamics 22 (10) (1993) 833–854. doi:10.1002/eqe.4290221002.